A New Ring-shape High Temperature Superconducting Trapped Field Magnet

Jie Sheng[1], Min Zhang[1]*, Yawei Wang[1], Xiaojian Li[1, 2], Jay Patel[1] and Weijia Yuan[1]

[1] Department of Electronic and Electrical Engineering, University of Bath， UK

[2] North Vehicle Research Institute, China

* corresponding author

E-mail: M.Zhang2@bath.ac.uk.

Abstract:

This paper presents a new type of trapped field magnet made of second generation high temperature superconducting (2G HTS) rings. This so-called ring-shape 2G HTS magnet has the potential to provide much stronger magnetic fields than existing permanent magnets. Compared to existing 2G HTS trapped field magnets, e.g. 2G HTS bulks and stacks, this new ring-shape 2G HTS magnet provides a promising technique to produce lager dimension magnets for industrial applications. This paper focuses on the working mechanism of this new structure magnet, both experimental and numerical study based on commercial magnetization techniques were carried out. Unique features have been identified and quantified for this new type of HTS magnet in field cooling and zero field cooling process. The magnetization mechanism is explained from the view of shielding and penetration of external magnetic field. An accumulation in the trapped field was observed by using multiple pulse field cooling. Besides, three types of demagnetization were also studies to ensure the practical properties of the ring-shape magnets. Conclusions obtained in this paper shows that this new ring-shape HTS magnet is very promising in trapping high magnetic field. As a super permanent magnet, it will have impacts in large-scale industrial applications, e.g. developing HTS machines with very high power density.

Keywords: Trapped field magnet, 2G HTS ring, Magnetization, Demagnetization.

1. Introduction

Second generation high temperature superconducting (2G HTS) trapped field magnets have significant potential for a variety of engineering applications to provide strong magnetic field and replace conventional permanent magnets, e.g. samarium-cobalt and neodymium-iron-boron. Bulk, single grain RE–Ba–Cu–O ((RE)BCO, where RE is a rare-earth element) superconductors have been a research focus for more than twenty years. Using the top seeded melt growth (TSMG) process and reinforcement technique, the record trapped field have exceeded 17 T for a single grain YBCO bulk [1,2]. Multiple seeding technique has been used to increase the size of YBCO bulks [3,4,5]. The 2G HTS bulks have been demonstrated as trapped field magnets for electrical machines [6,7], as well as self-stabilising bearings for energy storage flywheels and magnetic separation devices [8,9]. The magnetization of 2G HTS bulks has been studied extensively, partly because it is one of the key challenges. Pulsed field magnetization (PFM) has been identified as an effective and practical way to magnetize 2G HTS bulks [10,11,12,13]. Due to the heat generated in the stack, the trapped field and flux acquired by PFM is usually less than that acquired by field cooling or zero field cooling methods, especially at lower temperatures [14,15]. Therefore, effort has been devoted to optimize the PFM process to improve the trapped field with PFM. Recent study has shown higher trapped field can be achieved using flux jump-assisted PFM or using slit coils [16,17]. Thermally coupled numerical models have been developed to simulate the trapped field during PFM process and study the influence of grain boundaries [18,19].

More recently, with the maturing of YBCO coated conductor technology, stacks of YBCO tapes have been proposed as a new type of trapped field magnet with a maximum trapped field of 7 T reported [20,21]. Compared to the melt-processed bulks, it is relatively easier to make a stack of YBCO tapes and control their quality. PFM and flux pumping for a stack of YBCO tapes has been demonstrated [22]. Modelling of the stack of YBCO tapes has been reported taking into account the effect of stabilizers [23,24]. Both types of HTS trapped field magnets have a limitation in sizing. The diameter of single grain 2G HTS bulks is usually less than 40 mm while the maximum width of stack of YBCO tapes is the width of commercial YBCO coated conductors (46 mm).

This paper reports a new type of 2G HTS trapped field magnet, which is called ring-shape 2G HTS magnet. As shown in Fig.1, by splitting 2G HTS coated conductors, shaping them into a ring-shape and stacking them into a magnet, the ring-shape 2G HTS magnet can be easily constructed. The main advantage of the new magnet is that it can be feasibly sized. By choosing different length of the split, we can adjust the diameter of the magnet. This ring-shape 2G HTS was inspired by the wind-and-flip method, which was used to construct joint-less 2G HTS coils for NMR/MRI applications [25,26,27,28,29] and fault current limiters [30,31]. Instead of using one piece of YBCO conductor to wind into coils and applying a DC current, our ring-shaped trapped field magnets use stacks of ring-shape YBCO conductors [32], The trapped field comes from induced persistent current loops using conventional magnetization methods, e.g. field cooling, zero field cooling and pulsed magnetization.

Due to the difference in geometry, the magnetization of the ring-shape magnet can be understood by neither Bean model nor the existing knowledge obtained from the study on 2G HTS bulks and stack of tapes. Therefore, this paper presents, for the first time, a thorough study of the ring-shape HTS magnet, with particular focus on the magnetization and demagnetization mechanism. We employed both experimental method and numerical modelling to unveil the electromagnetic performance of the new magnet. The paper is organized as follows: section two presents the magnetic field distribution of the magnet and our experimental setup; section three focuses on three types of magnetization for the ring-shape magnets: field cooling, zero field cooling and multiple pulse field cooling; section four focuses on the demagnetization process of the magnets.

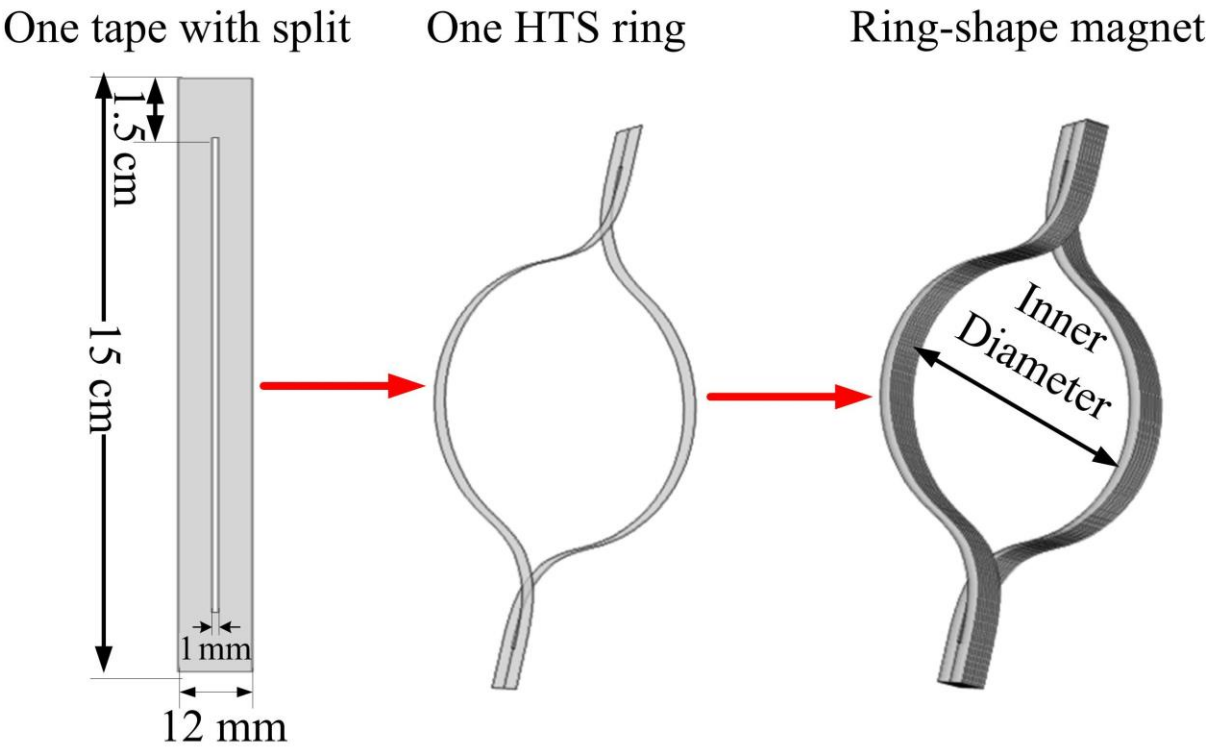

Figure 1. The construction of the ring-shape YBCO magnets.

2. Experimental setup and modelling

2.1. Magnet construction and magnetic field mapping

Figure 1 illustrates the construction process of our sample ring-shape 2G HTS magnet. 15 cm long YBCO tapes (12 mm wide, self-field critical current 317 A in 77 K, manufactured by Superpower) were split by mechanical cutting. The split opening in the centre of the tape is 120 mm in length and 1mm in width, with 15 mm spare tape at each end. Nine YBCO rings are stacking together to form the magnet and a round G10 former was inserted into the ring opening (diameter 50 mm) to maintain the ring-shape.

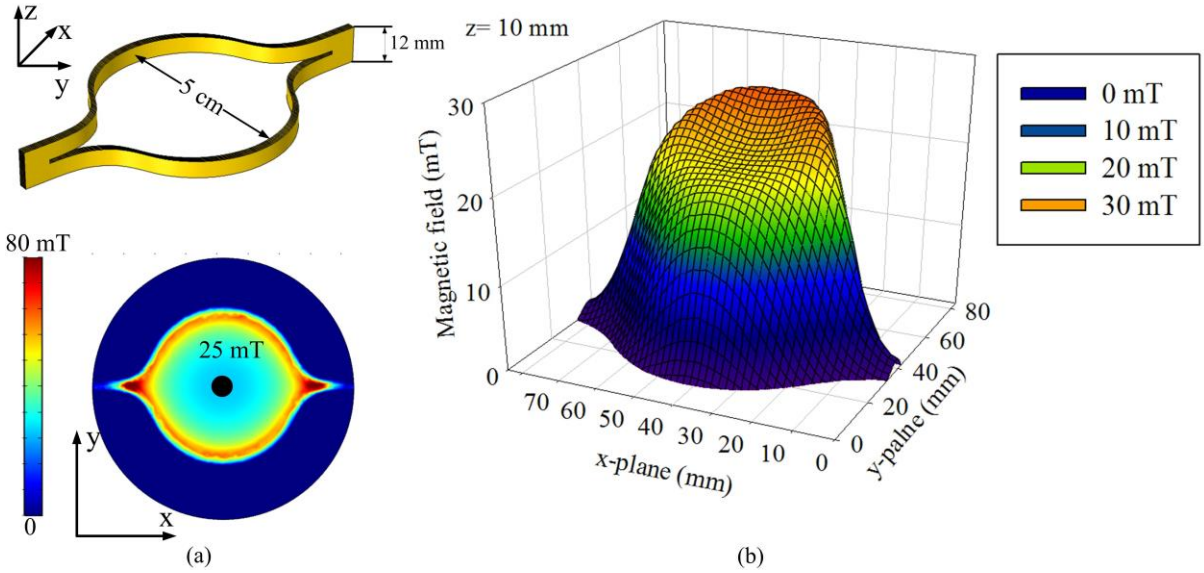

Figure 2. Magnetic field distribution (Bz) of the sample magnet when it is fully penetrated: (a) centre plane z = 0 mm; (b) z= 10mm The sample coil has an inner diameter of 5 cm. The trapped field is in z directions.

Figure 2 shows the theoretical magnetic field distribution of the ring-shape YBCO magnet with maximum trapped field in 77K obtained by a 3D real size model. The trapped field in the centre plane (z = 0 mm) is shown in Fig. 2 (a). The central fully trapped field is 25 mT, which is defined as B_p (full penetration field density) for following discussions. Fig. 2 (b).plots the magnetic field density Bz 4 mm above the magnet (z = 10 mm). Due to the asymmetric geometry on the axial direction, the ring-shape magnet has an angle deflection of the trapped magnetic field. This angle deflection leads to asymmetric magnetic field distributions. In this case, the upper bar generates a magnetic field about 10 mT higher than the central field. A strategy to reduce the field asymmetry has been proposed using double split structure [33]. In this case, we focus on the single split structure as shown in Fig.1.

2.2. Experiment

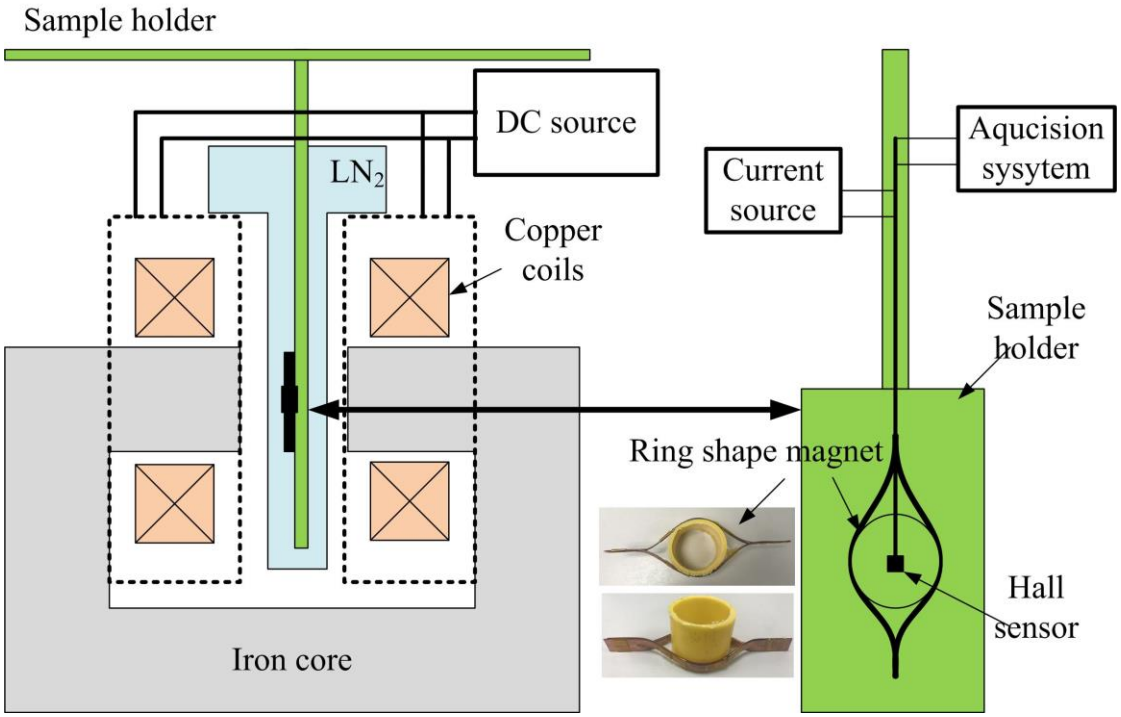

Figure 3. The magnetization test rig for the ring-shape YBCO magnet.

Figure 3 shows our testing rig, which consists of an iron-core based DC magnet to provide the external magnetic field, a sample holder to support the ring-shape magnet, a calibrated low-temperature hall sensor and NI data acquisition system. The DC magnet can provide a uniform magnetic field in the central air gap; amplitude of the magnetic field can be manually set to a value between 0 to 0.4 T. The magnet can be programmed to achieve different kinds of waveforms with a minimum time step of 1 s. The HHP-NP hall sensor (*error* < 0.2% below 1 T) is placed in the centre of the magnet. To magnetize the ring-shape magnet, we use three methods: field cooling (FC), zero field cooling (ZFC) and multiple pulse field cooling (MPC). We control the DC power supply of the copper magnet to achieve these three magnetization methods. Fig.4 illustrates the difference among FC, ZFC and MPC. For FC, we apply an external magnetic field, gradually cool down the ring-shape magnet, and then remove the external field. For ZFC, we cool down the magnet first, and apply a positive pulse field waveform with different magnitudes. For MPC, we repeat the positive pulse field waveform. The magnetic field of the magnet centre was measured during the magnetization processes.

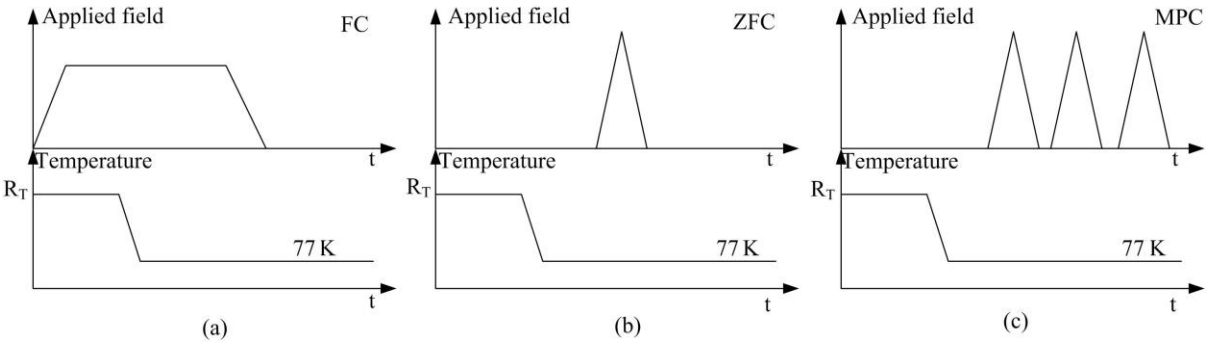

Figure 4. Three different magnetization processes: (a) field cooling (FC); (b) zero field cooling (ZFC); (c) multiple pulse field cooling (MPC)

2.3. Finite element model

To model the ring-shape YBCO magnet in the finite element software Comsol in an effective way, we use previously validated 2D axial symmetrical H formulation [34,35,36]. The governing equation is shown in Equ.1:

$$\mu_0\mu_r \frac{\partial H}{\partial t} + \nabla \times (\rho \nabla \times H) = 0 \qquad (1)$$

where $\mathbf{H}$= [$\mathbf{H}_r$; $\mathbf{H}_z$] is the magnetic field, ρ is the resistivity. For air, we use ρ = 1000 Ωm; for YBCO, we use the *E-J* power law:

$$\rho = E_0 / J_c(B) \times (J_\varphi / J_c(B))^n \qquad (2)$$

where n = 30, E_0 = 100 μV/m and $J_c(B)$ is the field-dependent critical current of YBCO [38]. Only the 1 μm thick YBCO layer is modelled to represent the YBCO ring. Since the 12 mm YBCO conductor was split into two, each YBCO ring is 5.5 mm wide. The distance between two rings is the thickness of the YBCO conductor, which is 100 μm. From a 2D cross section view, the ring closest to symmetrical axis is ring 1, while the outermost ring is ring 9.

3. Magnetization study

3.1. Field cooling and zero field cooling.

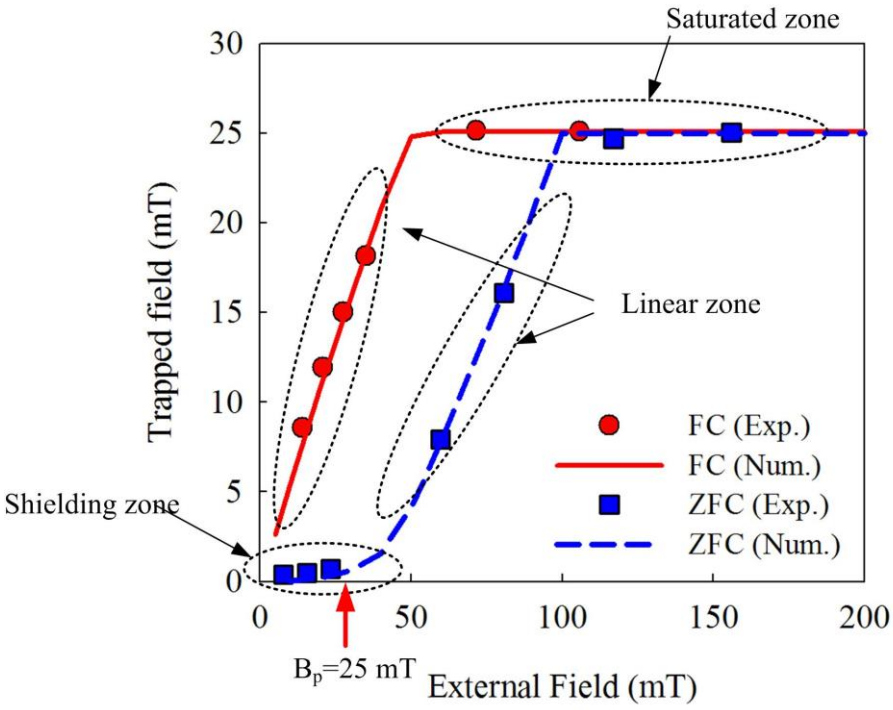

Figure 5. Experimental and numerical results of the sample ring-shape magnet based on FC and ZFC, where the ring diameter is 50 mm, and the effective HTS width is 5.5 mm for the ring.

Figure 5 shows the results of FC and ZFC. The modelling results match well with experimental measurements, indicating that the 2D axial symmetrical model is a good representation for the ring-shape magnet. The FC process of the ring-shape YBCO magnet is similar to YBCO bulks and stack of tapes. The trapped field increases linearly with the amplitude of applied field before the magnet is fully penetrated. The maximum tapped field is 25 mT (B_p = 25 mT) with an applied field of 50 mT, which matches our field mapping modelling results in Fig.2. The trapped field rate is about 50% (trapped field rate = max trapped field/applied field). Further increase of the applied field doesn't affect the trapped field because the ring-shape magnet has entered the saturated zone.

For YBCO bulks and stack of tapes, when the applied field is below B_p, the final trapped field equals the applied field. The trapped field rate is 100% in theory. But for the ring-shape HTS magnet in the FC process, the trapped field rate varies. Our study indicates that the trapped field rate of the

ring-shape magnet is affected by both the inner diameter of the magnet and the HTS tape width. Figure 6 (a) shows how the HTS tape width affects the FC trapped field rate. Basically the wider the tape, the higher the trapped field rate. The readers are reminded that the tape width mentioned here is not the width of the YBCO tape being cut. Instead, it is defined as the width of the ring bar. In this case, it is 5.5 mm due to 1 mm split loss in the centre, corresponding to a trapped field rate of 50%. If a 40 mm HTS tape is used to build the ring-shape magnet, the trapped field rate can reach 80% on the assumption that the inner diameter of the magnet is 5 cm. Figure 6 (b) shows how the trapped field rate changes with the inner diameter of the magnet. The larger the magnet diameter, the lower the trapped field rate. The maximum trapped field rate can be 100% when the inner diameter is smaller than 1 cm.

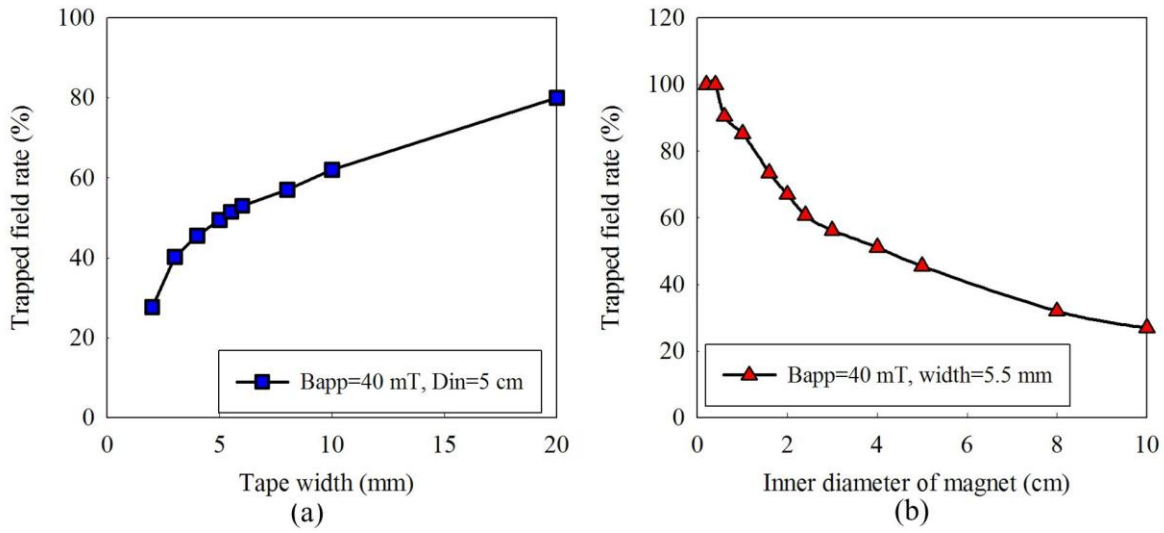

Figure 6. Trapped field rate of the ring-shape magnet in FC process: (a) influence of the tape width (the inner diameter of the magnet is 5 cm); (b) influence of the inner diameter of the magnet (the HTS tape width is 5.5 mm).

ZFC result in Fig.5 shows a more unique feature of the ring-shape magnet. It was noticed that there are three zones in the ZFC process according to the magnitude of the applied field. When the applied field is smaller than B_p (25 mT in this case), there is the shielding zone which sees nearly zero trapped fields. This is because the applied field was fully shielded by the YBCO ring so the magnet centre sees and traps very small magnetic fields. When the applied field is higher than B_p, it enters the

linear zone where the final trapped field increases linearly with the increase of the applied field. When the applied field reaches four times the B_p, it is the saturation zone where the trapped field remains as B_p.

To help understand the uniqueness of the three ZFC zones, current distributions of each YBCO ring during the ZFC process are plotted in Fig.7. For an applied field of 10 mT, the outermost ring (ring 9) and the second outermost ring (ring 8) has opposite current directions, which is the reason that nearly zero trapped field was measured at the centre of the magnet. The opposite current directions suggest that there is a shielding effect due to the applied magnetic field. Therefore it is called the shielding zone ($B_{apply} < B_p$). A similar situation is found for the applied field of 20 mT. When B_{apply} is higher than B_p, it enters the linear zone where we start to see fully penetrated rings. For example, with the applied field of 30 mT, the outermost ring (ring 9) is fully penetrated while ring 8 and ring 1 are half penetrated. The rest of the rings are still in the shielding status. Further increase of the applied field sees more rings enter the fully penetrated or half penetration status, which results in an increase in the trapped field. When B_{apply} exceeds 100 mT (four times the B_p), all YBCO rings are fully penetrated with the same current distribution, which is the so-called saturated zone.

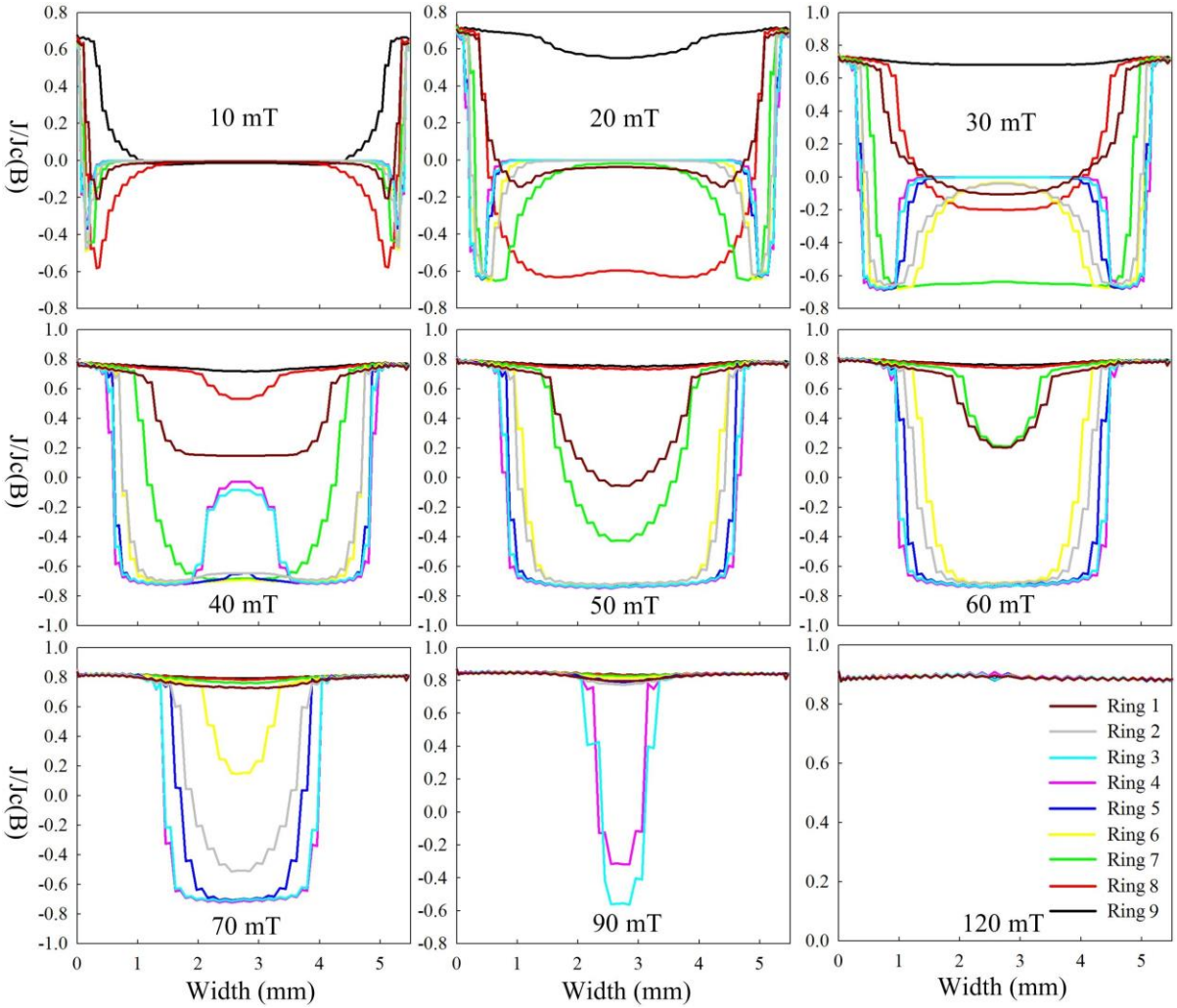

Figure 7. Calculated current distributions of all YBCO rings during ZFC. Applied field 10 mT and 20 mT belong to the Shielding zone, 30-90 mT belongs to the Linear zone, and 120 mT belongs to the Saturated zone.

3.2. Multiple pulse field cooling

The multi-pulse magnetization techniques have been experimentally proved to improve the trapped field of HTS bulk effectively. The multi-pulse techniques include successive pulsed-field application (SPA), iteratively magnetizing pulsed field method with reducing amplitude (IMRA), and multi-pulse technique with step-wise cooling (MPSC)[37, 38]. We performed MPC tests for our ring-shape YBCO magnet. As explained previously, there are three zones in the ZFC process based on the magnitude of the applied field. So we did three MPC tests with the applied field in the shielding, linear and saturated zones respectively. The experimental results are shown in Fig.8.

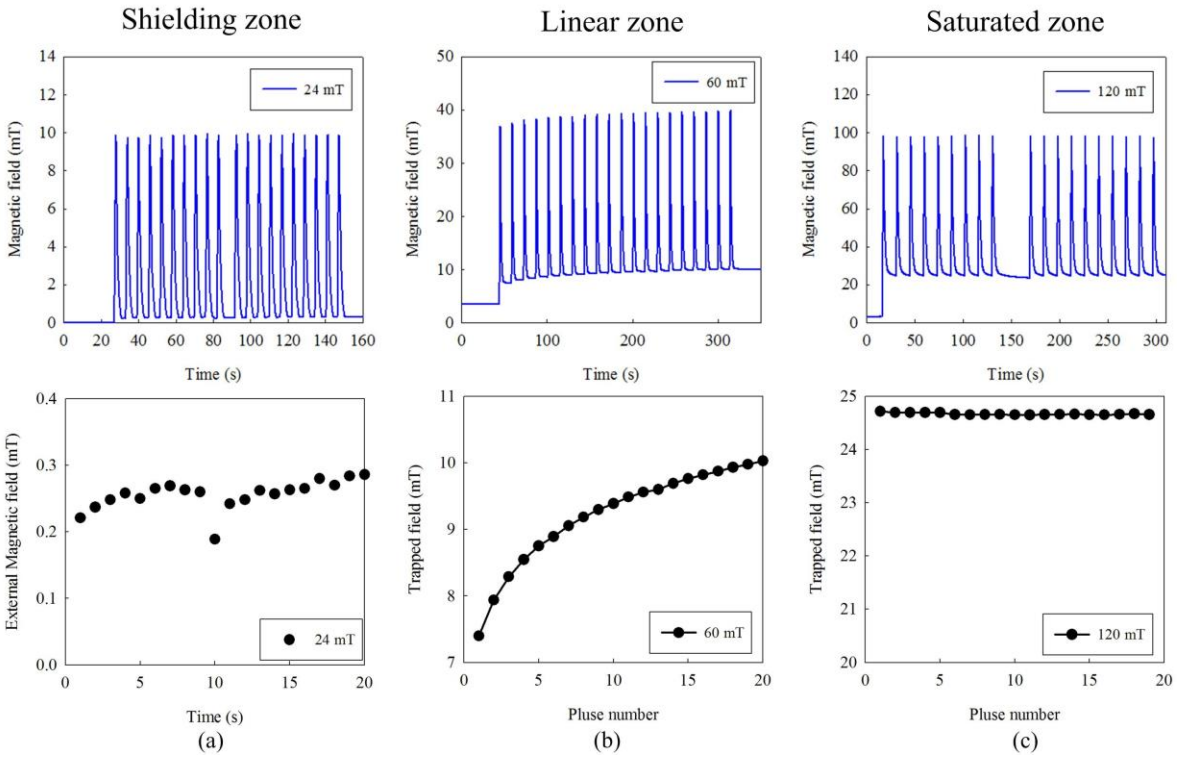

Figure 8. Measured magnetic fields in the MPC process: (a) Shielding zone MPC, applied field 24 mT; (b) Linear zone MPC, applied field 60 mT; (c) Saturated zone MPC, applied field 120 mT.

Figure 8 shows the measured magnetic field (trapped field from the ring plus the applied field) during the MPC process. The applied field is a programmed triangular pulse with controllable ramping up rates (0-120 mT/s) and a constant ramping down rate (18 mT/s).

Figure 8 (a) shows the MFC process with an applied field in the shielding zone (24 mT). As discussed previously, the trapped field is very small (0.2-0.3 mT). Fig. 8 (b) shows the trapped field increases during the MPC process with an applied field in the linear zone. In 20 pulse cycles, the trapped field increases from 7.3 mT to 10 mT. The increase rate slows down with the increase of pulse cycles. Fig. 8 (c) shows the trapped field saturates during the MPC process with an applied field in the saturated zone. We notice a small decline of the trapped field, which is due to the flux creep.

We are interested in the accumulation of the trapped field in the linear zone, which indicates that a relatively small applied field can be used to magnetize the ring-shape magnet in the MPC process to gradually build up the trapped field. To further understand the reason behind this accumulation, we plot the current distributions of each YBCO ring during the MPC process. With an applied field of

60 mT, ring 8 and ring 9 (outermost two rings) are fully penetrated, so their current distributions show little changes in the MPC process. Ring 1 and ring 7 are half penetrated after the first pulse cycle, and the penetration areas gradually increase in the following pulse cycles. After the 5th pulse cycles, ring 1 and ring 7 become fully penetrated, and their current stays the same for the subsequent pulse cycles. Starting from the 5th pulse cycle, the applied field starts to penetrate to ring 2 and ring 6. Therefore the currents in ring 2 and 6 start to increase. This continuously penetration by MFC leads to the accumulation of total currents flowing in the magnet, which leads to the accumulation of the trapped field.

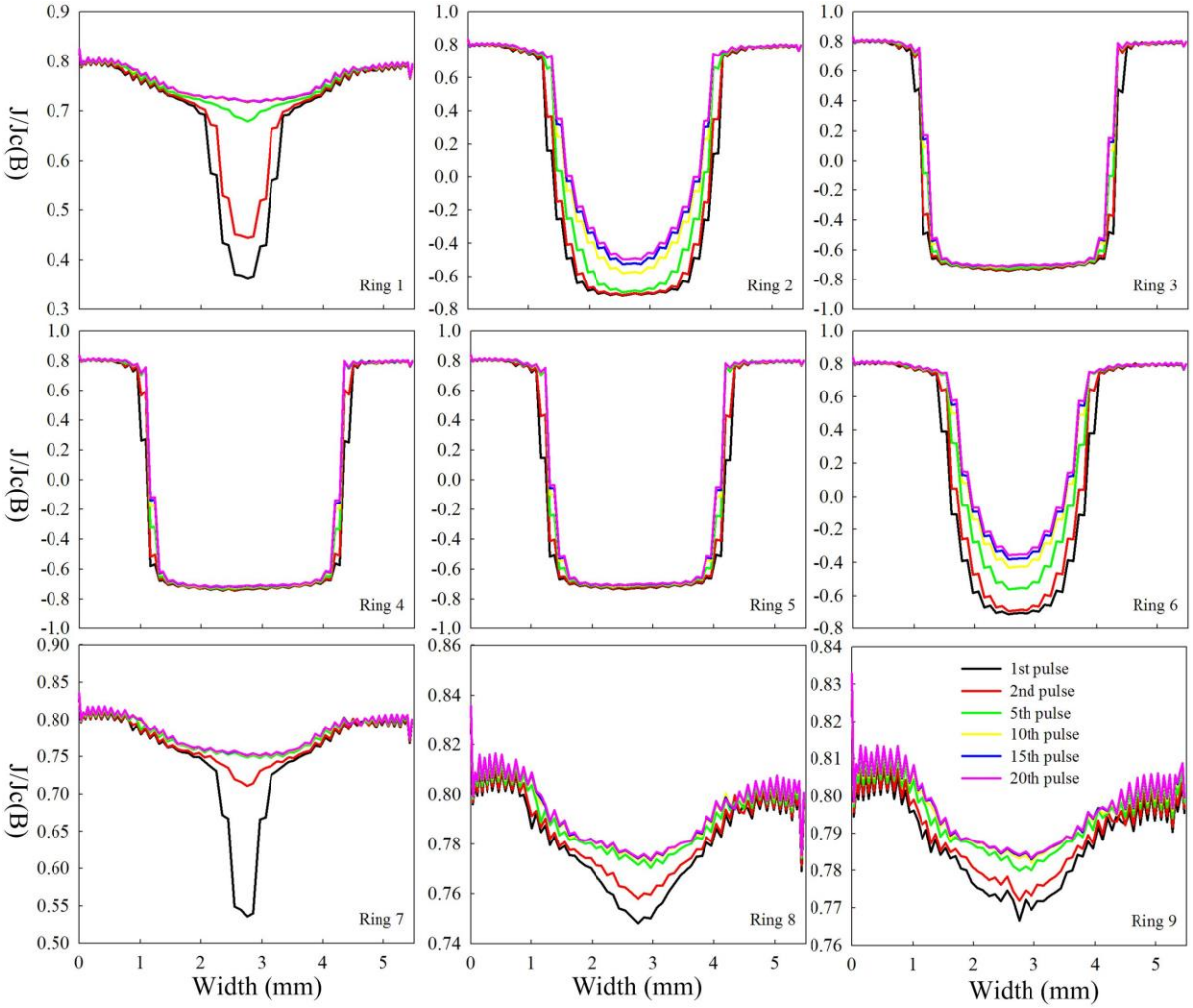

Figure 9. Calculated current penetration in the YBCO rings during the MPC process with applied field of 60 mT.

4. Demagnetization

Demagnetization is an important issue for the application of HTS trapped field magnet. For practical applications, the demagnetization rates of trapped field magnets need to be estimated to determine whether or not re-magnetization is required. The demagnetization of 2G HS bulks and stack of YBCO tapes have been studied extensively, with both perpendicular and parallel magnetic fields [39,40,41,42]. Strategies to suppress the demagnetization have been proposed using shielding rings [43,44].

Here we report the demagnetization measurements of the ring-shape YBCO magnet. Figure 10 illustrates the three directions of the demagnetization field applied to the sample. Figure 10 (a) shows the positive perpendicular field demagnetization (demagnetization field is perpendicular to the ring plane). Positive demagnetization indicates that the demagnetization field is in the same direction as the trapped field. Figure 10 (b) shows the negative perpendicular field demagnetization. Negative demagnetization indicates that the demagnetization field is in the opposite direction as the trapped field. This is a very common situation in HTS machine applications, where the ring magnet provides the rotor magnetic field while the demagnetization field comes from the stator current. Figure 10 (c) shows the parallel demagnetization where the demagnetization field is in parallel direction to the ring plane.

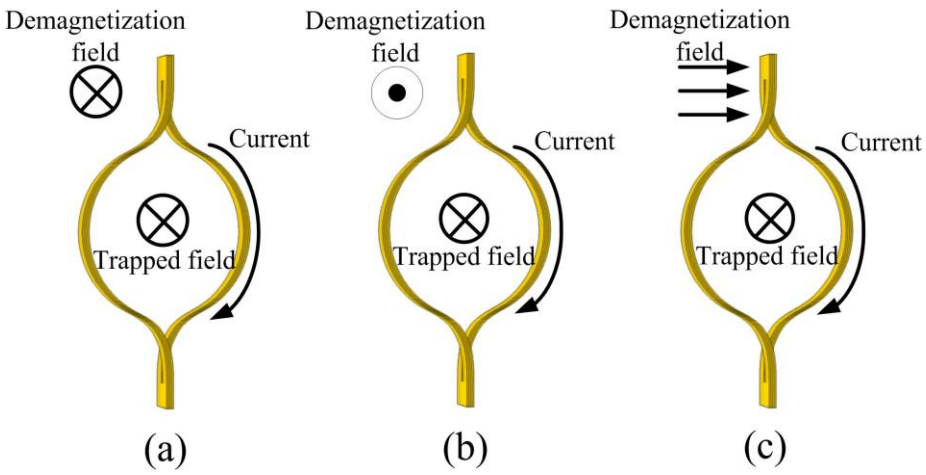

Figure 10. Three types of demagnetization: (a) positive perpendicular demagnetization; (b) negative perpendicular demagnetization; (c) parallel demagnetization.

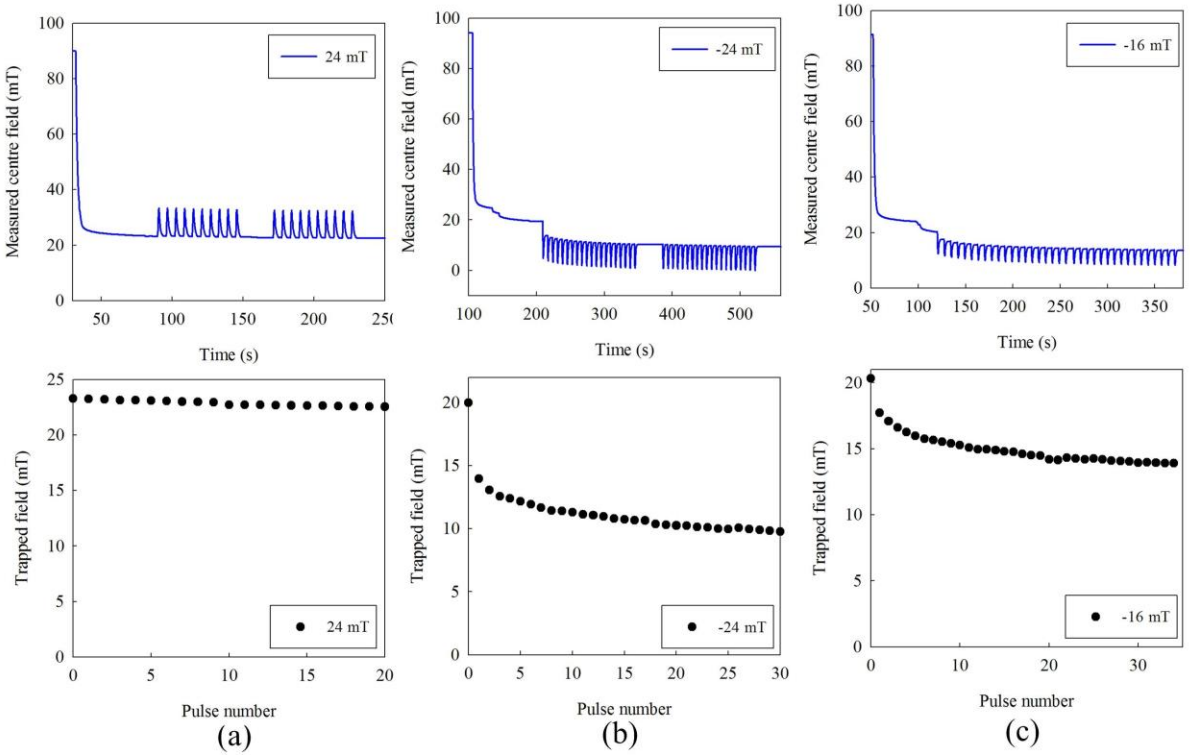

Figure 11. The measured trapped fields of the sample in perpendicular demagnetization: (a) positive demagnetization with 24 mT magnetic field; (b) negative demagnetization with 24 mT magnetic field; (c) negative demagnetization with 16 mT magnetic field

Figure 11 (a) shows the measured magnet field in the magnet centre and the trapped field in a positive perpendicular demagnetization process. The trapped field is not affected by demagnetization, because the slight decay rate of the trapped field is due to the flux creep in HTS rings. Figure 11 (b) and (c) show the measured magnet field in the magnet centre and the trapped field in negtive perpendicular demagnetization processes, where the demagnetisation field is in opposite direction to the trapped field. Both cases show a certain degree of demagnetization. The demagnetization effect of the first cycle is the strongest and then it gradually reduces. As shown in Fig. 11 (b) and (c), the first demagnetization cycle forced the trapped field to drop by a ratio of 27% and 11.5% respectively. In comparison. the subsequent 29 demagnetization cycles forced the trapped field to drop by a ratio of 24.2% and 19% respectively .

To understand the mechanism of demagnetization, we plot the current distributions in each ring based on a 24 mT negative perpendicular demagnetization (9 cycles in total), as shown in Fig. 12. The magnet is fully penetrated before the demagnetization; therefore all the HTS rings have the same

current distribution (the black line). In the first demagnetization cycle, all the HTS rings see a significant reduction in currents, corresponding to the sharp drop of the trapped field. From the second cycle, only the outermost rings (ring1, 8, 9) show current reductions, because they serve as the shielding layers for the middle rings. That explains why the demagnetization effect slows down after the first cycle.

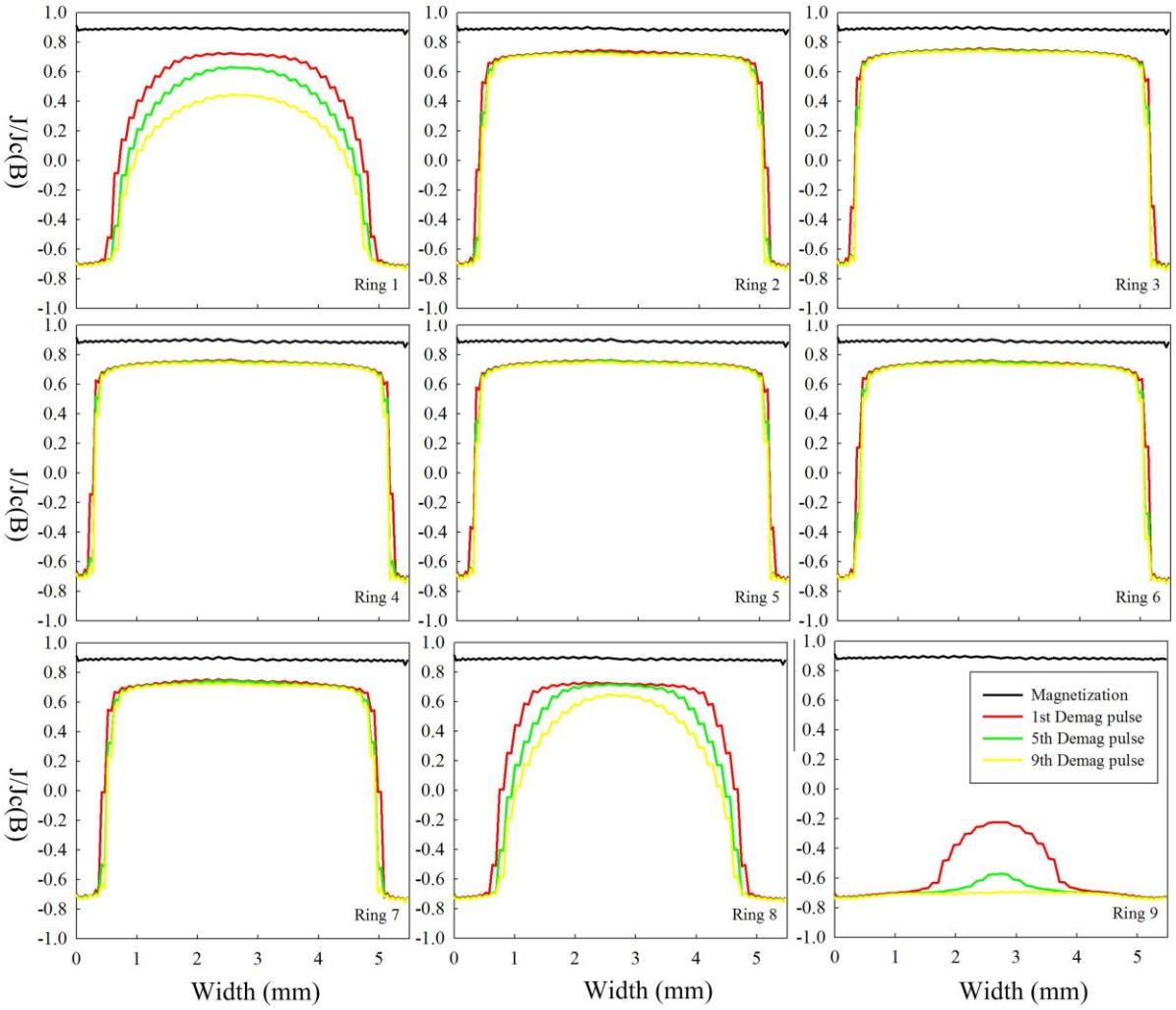

Figure 12. Calculated current distributions in the YBCO rings during a 24 mT negtive perpendicular demagnetization process.

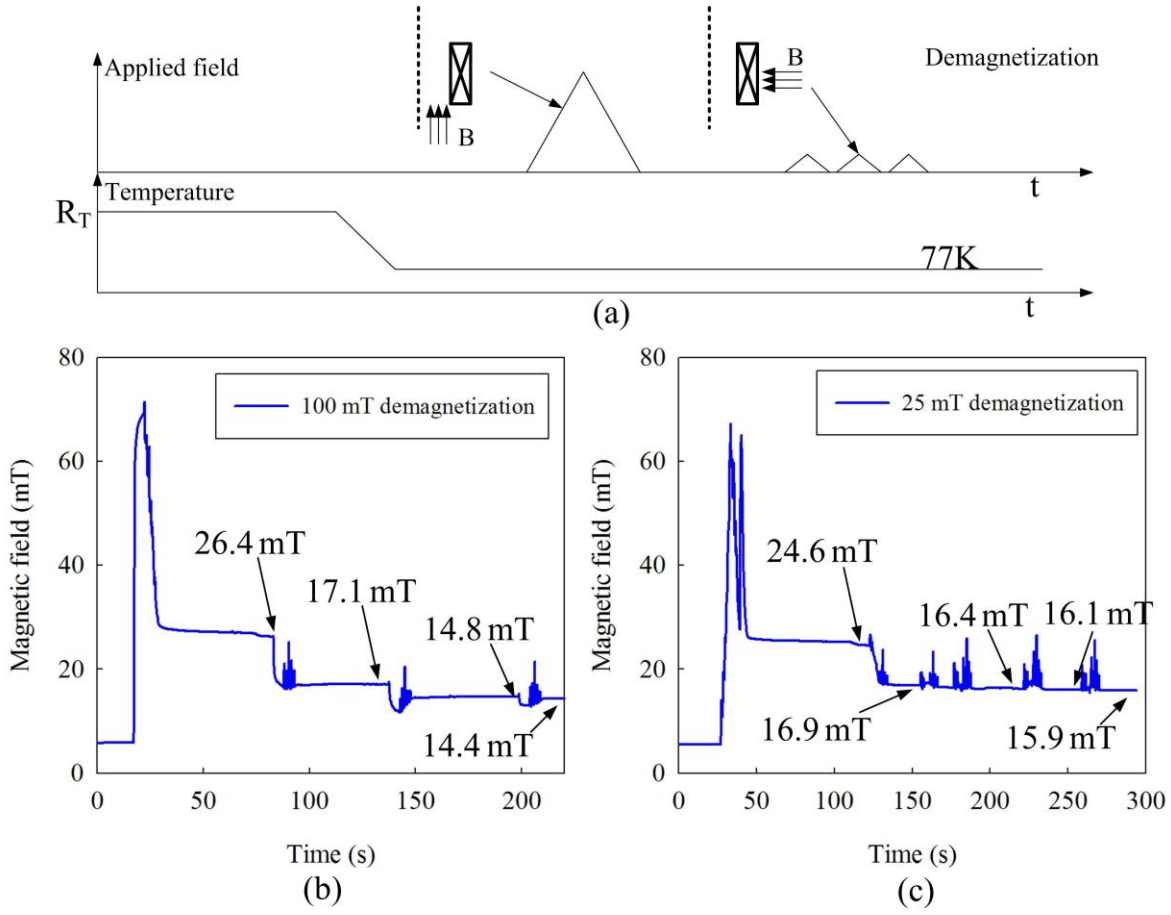

Figure 13. Parallel demagnetization process of the sample with different field magnitudes: (a) the experiment process; (b) measured magnetic field with 100 mT parallel field; (c) demagnetization with 25 mT parallel field.

Figure 13 (a) shows the experimental procedure of a parallel demagnetization process. The ring-shape magnet was firstly magnetized by a ZFC to a fully penetration status. Then the sample holder was rotated by 90 degrees, so that the applied field is parallel to the ring plane. The demagnetization was then carried out by applying multiple triangular waveforms.

Figure 13 (b) and (c) show the measured centre magnetic fields with 100 mT and 25 mT parallel demagnetization respectively. When the first cycle of the 100 mT parallel field is applied, the trapped field decreases from 26.4 mT to 17.1 mT by a ratio of 35%. It then gradually dropped by 8.7% in the second and third cycle respectively. The demagnetization rate slows down with the increase of demagnetization cycles. As shown in Fig. 13 (c), after a 31.3% drop in trapped field in the first demagnetization cycle, the trapped field further decreases only 4% in the next three cycles. Theoretically, the parallel demagnetization field is perpendicular to the HTS tape surface. So current loops in the a-b plane can be induced in the outermost HTS rings to shield the demagnetization field,

leading to a complete rearrangement of current in the outermost rings and a significant reduction of the trapped field during the first demagnetization cycle.

5. Conclusion

This paper reported our latest study on a new type of 2G HTS trapped field magnet, the so-called ring-shape magnet. The new magnet is very promising in large-scale applications to replace permanent magnets, e.g. HTS trapped field machines, MRI devices. As the fundamental study paper, this paper focuses on the magnetization and demagnetization mechanisms of the new magnet, and tries to prove its great potential properties for the industrial applications. Unique features in magnetization have been identified and quantified for this new type of HTS magnet, and hopefully can be used as a guideline of industrial magnetization techniques. Our findings can be summarised as:

- In FC study, it is identified that the percentage of applied magnetic field that can be trapped in our sample is 50%, and can be further improved to nearly 100% by modifying the tape width and inner diameters.

- In ZFC study, it is identified that there are three different zones based on the relationship between the applied field and the trapped field, namely the shielding zone, linear zone and saturated zone. Flux accumulation effect was observed in linear zone using MFC methods, which provides a possible way to magnetize the magnets by a relative small external magnetic field.

- In the demagnetization study, the new magnet is subjected to a significant trapped field reduction during the first cycle of demagnetization. Because individual HTS rings are used to construct the magnet, the outermost and innermost rings serve as shielding layers to the demagnetization field, which help to slow down the demagnetization rate in the subsequent cycles.

Acknowledgments

Dr Min Zhang thanks the supports from the EPSRC Grant EP/P002277/1 and the Research Fellowship of Royal Academy of Engineering.

Reference

[1] Tomita M and Murakami M 2003 High-temperature superconductor bulk magnets that can trap magnetic fields of over 17 tesla at 29 K Nature 421 517–520

[2] Durrell J H, Dennis A R, Jaroszynski J, Ainslie M D, Palmer K G B, Shi Y H, Campbell A M, Hull J, Strasik M, Hellstrom E E and Cardwell D A 2014 A trapped field of 17.6 T in melt-processed, bulk Gd-Ba-Cu-O reinforced with shrink-fit steel Supercond. Sci. Technol. 27 082001

[3] Todt V R, Zhang X F, Miller D J, St Louis-Weber M and Dravid V P 1996 Controlled growth of bulk bicrystals and the investigation of microstructure - property relations of YBa2Cu3Ox grain boundaries Appl. Phys. Lett. 69 3746

[4] Ida T, Li Z, Zhou D F, Miki M, Zhang Y F and Izumi M 2016 Materials preparation and magnetization of Gd-Ba-Cu-O bulk high-temperature superconductors Supercond. Sci. Technol. 29 054005

[5] Kim C-J, Kim H-J, Joo J-H, Hong G-W, Han S-C, Han Y-H, Sung T-H and Kim S-J 2000 Effects of the seed distance on the characteristics of the (100)/(100) junctions of top-seeded melt growth processed YBCO superconductors using two seeds 2000 Physica C 336 233

[6] Huang Z, Zhang M, Wang W and Coombs T A, 2014. Trial test of a bulk-type fully HTS synchronous motor. IEEE Trans. Appl. Supercond. 24 4602605

[7] Matsuzaki H, Kimura Y, Ohtani I, Izumi M, Ida T, Akita Y, Sugimoto H, Miki M and Kitano M 2005 An axial gap-type HTS bulk synchronous motor excited by pulsed-field magnetization with vortex-type armature copper windings IEEE Trans. Appl. Supercond. 15 2222 - 2225

[8] Hull J R and Murakami M 2004 Applications of bulk high temperature superconductors Proc. IEEE 92 1705–1718

[9] Oka T, Hirayama E, Kanai T, Ogawa J, Fukui S, Sato T, Yokoyama K and Nakamura T 2014 Strong magnetic field generator containing HTS bulk magnets and compact refrigerators IEEE Trans. Appl. Supercond. 24 1–4

[10] Yokoyama K, Oka T and Noto K 2011 Evaluation of pulsed-field magnetization on a superconducting bulk magnet system using a 13 K refrigerator IEEE Trans. Appl. Supercond. 21 1657–1660

[11] Oka T, Seki H, Ogawa J, Fukui S, Sato T and Yokoyama K 2011 Performance of trapped magnetic field in superconducting bulk magnets activated by pulsed field magnetization IEEE Trans. Appl. Supercond. 21 3356-3359

[12] Fujishiro H, Naito T, Kakehata K, Yanagi Y and Itoh Y 2010 Estimation of temperature rise from trapped field gradient on superconducting bulk magnetized by multi-pulse technique Supercond. Sci. Technol. 23 025013

[13] Fujishiro H, Kawaguchi S, Kaneyama M, Fujiwara A, Tateiwa T and Oka T 2006 Heat propagation analysis in HTSC bulks during pulse field magnetization Supercond. Sci. Technol. 19 S540-S544

[14] Fujishiro H, Oka T, Yokoyama K and Noto K 2003 Time evolution and spatial distribution of temperature in YBCO bulk superconductor after pulse field magnetizing Supercond. Sci. Technol. 16 809-814

[15] Fujishiro H, Kaneyama M, Yokoyama K, Oka T and Noto K 2004 Generated heat during pulse field magnetizing for REBaCuO (RE= Gd, Sm, Y) bulk superconductors with different pinning abilities Supercond. Sci. Technol. 18 158-165

[16] Zhou D, Ainslie M D, Shi Y, Dennis A R, Huang K, Hull J R, Cardwell D A and Durrell J H 2017 A portable magnetic field of >3 T generated by the flux jump assisted, pulsed field magnetization of bulk superconductors Appl. Phys. Lett. 110 062601

[17] Ainslie M D, Fujishiro H, Mochizuki H, Takahashi K, Shi Y H, Namburi D K, Zou J, Zhou D, Dennis A R and Cardwell DA 2016 Enhanced trapped field performance of bulk high-temperature superconductors using split coil, pulsed field magnetization with an iron yoke Supercond. Sci. Technol. 29 074003

[18] Zhang M, Matsuda K and Coombs T A 2012 New application of temperature-dependent modelling of high temperature superconductors: Quench propagation and pulse magnetization J. Appl. Phys. 112 043912

[19] Ainslie M D and Fujishiro H 2015 Modelling of bulk superconductor magnetization Supercond. Sci. Technol. 28 053002

[20] Patel A, Filar K, Nizhankovskii V, Hopkins S C, Glowacki B A, 2013 Trapped fields greater than 7 T in a 12 mm square stack of commercial high-temperature superconducting tape Appl. Phys. Lett. 102 102601

[21] Tamegai T, Hirai T, Sun Y and Pyon S 2016 Trapping a magnetic field of 7.9 T using a bulk magnet fabricated from stack of coated conductors Physica C 530 20-23

[22] Zhang H, Geng J Z, Shen B Y, Fu L, Zhang X C, Li C, Li J, Tim A C 2017 Magnetization of Coated Conductor Stacks Using Flux Pumping. IEEE Trans. Appl. Supercond. 27 1-5

[23] Page A G, Patel A, Baskys A, Hopkins S C, Kalitka V, Molodyk A and Glowacki B A 2015 The effect of stabilizer on the trapped field of stacks of superconducting tape magnetized by a pulsed field Supercond. Sci. Technol. 28 085009

[24] Zou S N, Zermeno V and Grilli F 2016 Simulation of Stacks of High-Temperature Superconducting Coated Conductors Magnetized by Pulsed Field Magnetization Using Controlled Magnetic Density Distribution Coils IEEE Trans. Appl. Supercond. 26 1-5

[25] Kim W S, Lee S, Kim Y, Lee J Y, Park S H, Lee J K, Hong G W, Han J and Choi K 2015 Persistent Current Mode of a 1-T-Class HTS Pancake Coil for NMR/MRI Applications IEEE Trans. Appl. Supercond. 25 1-4

[26] Kosa J, Vajda I and Gyore A 2010 Application Possibilities with Continuous YBCO Loops Made of HTS Wire J. Phys.: Conf. Ser. 234 032030

[27] Lee H G, Kim J G, Lee S W, Kim W S, Lee S W, Choi K D, Honga G W and Ko T K 2006 Design and fabrication of permanent mode magnet by using coated conductor Physica C 445 1099-1102

[28] Lee S, Kim W S, Kim Y, Park S H, Lee J K, Hahn J H, Hong G W, Park I H, Park C and Choi K 2013 Characteristics of an HTS Pancake Coil in Persistent Current Mode Using Wind-and-Flip Winding Method IEEE Trans. Appl. Supercond. 23 4601305

[29] Levin G A, Barnes P N, Murphy J, Brunke L, Long J D, Horwath J and Turgut Z 2008 Persistent current in coils made out of second generation high temperature superconductor wire Appl. Phys. Lett. 93 062504

[30] Kosa J and Vajda I 2011 Novel 3-phase self-limiting transformer with magnetic flux applied by perfect closed YBCO wire loops IEEE Trans. Appl. Supercond. 21 1388-1392

[31] Kosa J, Vajda I, Gyore A and Kohari Z 2010 Fault current limiter with novel arrangement of perfect YBCO loops made of HTS wire Proc. Epe-Pemc T1069-T1073

[32] Rong C C, Barnes P N, Levin G A, Miller J D, Santosusso D J and Fitzpatrick B K 2015 Investigation of the relaxation of persistent current in superconducting closed loops made out of YBCO coated conductors IEEE Trans. Appl. Supercond. 25 8200805

[33] Qiu D, Wu W, Pan Y, Xu S, Zhang Z M, Li Z L, Li Z Y, Wang Y W, Wang L B, Zhao Y, Zhang Z W, Yang P, Hong Z Y and Jin Z J 2017 Experiment and numerical analysis on magnetic field stability of persistent current mode coil made of HTS-coated conductors IEEE Trans. Appl. Supercond. 27 1-5

[34] Zhang M, Yuan W, Kvitkovic J, Pamidi A 2015 Total AC loss study of 2G HTS coils for fully HTS machine applications Supercond. Sci. Technol. 28 115011

[35] Zhang M, Kim J H, Pamidi S, Chudy M, Yuan W and TA Coombs 2012 Study of second generation, high-temperature superconducting coils: Determination of critical current J. Appl. Phys. 111 083902

[36] Wang Y, Song H, Yuan W, Jin Z and Hong Z 2017 Ramping turn-to-turn loss and magnetization loss of a No-Insulation (RE) Ba2Cu3Ox high temperature superconductor pancake coil J. Appl. Phys. 121 113903

[37] Kamijo H and Fujimoto H 2001 Repeated pulsed-field magnetization with temperature control in a high-T/sub c/bulk superconductor IEEE Trans. Appl. Supercond. 11 1816-1819

[38] Fujishiro H, Hiyama T, Naito T, Yanagi Y and Itoh Y 2009 Enhancement of trapped field and total trapped flux on GdBaCuO bulk by the MMPSC+ IMRA method Supercond. Sci. Technol. 22 095006

[39] Berger K, Gony B, Douine B and Lévêque J 2016 Magnetization and demagnetization studies of an HTS bulk in an iron core IEEE Trans. Appl. Supercond. 26 4700207

[40] Baghdadi M, Ruiz H S, Fagnard J F, Zhang M, Wang W and Coombs T A 2015 Investigation of demagnetization in HTS stacked tapes implemented in electric machines as a result of crossed magnetic field IEEE Trans. Appl. Supercond. 25 6602404

[41] Campbell A, Baghdadi M, Patel A, Zhou D, Huang K Y, Shi Y and Coombs T A 2017 Demagnetisation by crossed fields in superconductors Supercond. Sci. Technol. 30 034005

[42] Vanderbemden P, Hong Z, Coombs T A, Denis S, Ausloos M, Schwartz J, Rutel I B, Babu N H, Cardwell D A and Campbell A M 2007 Behavior of bulk high-temperature superconductors of finite thickness subjected to crossed magnetic fields: Experiment and model Phys. Rev. B 75 174515

[43] Yamagishi K, Tsukamoto O and Ogawa J 2009 Suppression of influence of AC external magnetic field on trapped magnetic flux in the HTS bulk by use of HTS shielding rings IEEE Trans. Appl. Supercond. 19 3561–3564

[44]Yamagishi K, Tsukamoto O, Ogawa J and Miyagi D 2011 Study of method to suppress decay of trapped magnetic fluxes in the HTS bulk subjected to perturbation of external magnetic field by use shielding coil wound of HTS wire IEEE Trans. Appl. Supercond. 21 3320–3324